

L0-REGULARIZED HYBRID GRADIENT SPARSITY PRIORS FOR ROBUST SINGLE-IMAGE BLIND DEBLURRING

Ryan Wen Liu^{†,‡} Wei Yin[†] Shengwu Xiong[‡] Silong Peng[§]

[†]School of Navigation, Wuhan University of Technology, Wuhan 430063, China

[‡]Key Laboratory of Intelligent Perception and Systems for High-Dimensional Information of Ministry of Education, Nanjing University of Science and Technology, Nanjing 210094, China

[‡]School of Computer Science and Technology, Wuhan University of Technology, Wuhan 430070, China

[§]Institute of Automation, Chinese Academy of Sciences, Beijing 100190, China

ABSTRACT

Single-image blind deblurring is a challenging ill-posed inverse problem which aims to estimate both blur kernel and latent sharp image from only one observation. This paper focuses on first estimating the blur kernel alone and then restoring the latent image since it has been proven to be more feasible to handle the ill-posed nature during blind deblurring. To estimate an accurate blur kernel, L0-norm of both first- and second-order image gradients is proposed to regularize the final estimation result. The proposed L0-regularized hybrid gradient sparsity priors obtain major benefit from the intrinsic sparsity properties of images and can assist in guaranteeing high-quality blur kernel estimation. Once the blur kernel is estimated, the final clean image is robustly generated using the combination of L1-norm data-fidelity term and total variation regularizer. Experimental results have demonstrated the satisfactory performance of the proposed method.

Index Terms— image deblurring, deconvolution, sparsity, total variation, nonconvex nonsmooth optimization

1. INTRODUCTION

Single-image blind deblurring aims to simultaneously estimate blur kernel and latent sharp image from only one blurred observation, which is a typical ill-posed inverse problem. The blurred image B can be written as the convolution of a latent sharp image L with a *uniform* blur kernel k , i.e., $B = L * k + \epsilon$ with $*$ being the linear convolution operator. To eliminate the ill-posed nature, the statistical priors learned from blur kernels and clean images should be incorporated into the MAP estimation framework. Current blind deblurring methods are roughly separated into two types [1, 2, 3, 4]: (1) one-step methods that simultaneously estimate the blur kernel and latent sharp image; (2) two-step methods that first estimate the

blur kernel, and then restore the latent sharp image (i.e., *non-blind deconvolution*). The kernel size is often smaller than the image size. Thus, the simultaneous estimation of blur kernel and clean image often fails in practice [1, 2]. In contrast, the estimation of blur kernel alone is considerably more robust compared with the simultaneous version. This paper mainly focuses on the two-step method since it is more feasible to handle the ill-posed nature. The general MAP framework for blur kernel estimation is given by

$$\min_{k,L} \{ \mathcal{D}(L, k, B) + \lambda \Phi_L(L) + \gamma \Phi_k(k) \}, \quad (1)$$

where λ and γ are pre-defined positive regularization parameters, $\mathcal{D}(L, k, B)$ is the data-fidelity term, $\Phi_L(L)$ and $\Phi_k(k)$ respectively represent the regularization terms on latent image and blur kernel. The squared L2-norm version of $\mathcal{D}(L, k, B)$ is more common in current literature due to the assumption of Gaussian distributed noise. Both L1-norm [8] and squared L2-norm [5] versions of $\Phi_k(k)$, i.e., $\|k\|_1$ and $\|k\|_2^2$, perform well in accurately estimating blur kernels. Thus, much more attention has been paid to $\Phi_L(L)$ related to image sparsity priors. For example, total variation (TV) prior [6] and its logarithmic version [7] have been introduced. The pioneering normalized gradient sparsity prior [8], dark channel prior [9] and hybrid bright-dark channel prior [10] have achieved great success. Recently, the L0-norm of image gradients [5, 11, 12, 13], the ideal sparsity-promoting prior, has been selected to enforce the estimation accuracy. Patch-based low-rank prior [14] has also been successfully extended to blind deblurring. From a computational point of view, the low-rank-guided method easily suffers from high computational cost in practical applications.

Motivated by the L0-regularized blur kernel estimation [5, 11, 12], we proposed the hybrid gradient sparsity priors to further enhance the estimation accuracy by combining the L0-norm of both first- and second-order image gradients. Current research has demonstrated the effectiveness of the first- and second-order image gradients. Their combination [15, 16] has also been widely studied and achieved superior performance

This work was supported by the NSFC (No.: 51609195), and the Open Project Program of Key Laboratory of Intelligent Perception and Systems for High-Dimensional Information of Ministry of Education (No.: JYB201704).

compared with the single version. It is well known that L0-norm works well in naturally interpreting the sparsity of image gradients. Thus, it is necessary to combine the L0-norm of both first- and second-order image gradients to guarantee high-quality estimation. In particular, the L0-regularized hybrid gradient sparsity priors introduced in this work are able to better preserve the gradient sparsity and salient edges.

2. ROBUST BLUR KERNEL ESTIMATION

2.1. Blur Kernel Estimation Model

For the sake of computational efficiency, the squared L2-norm constraint on blur kernel (i.e., $\|k\|_2^2$) is directly utilized in this paper. Effectiveness of this convex constraint has been demonstrated [5, 11, 14]. Let $\nabla = \{\partial_x, \partial_y\}$ and $\Delta = \{\partial_{xx}, \partial_{xy}, \partial_{yx}, \partial_{yy}\}$ denote the first and second-order differential operators, respectively. As discussed in Section 1, the blur kernel estimation model is proposed by combining the L0-regularized first- and second-order image gradients

$$\min_{k, \nabla L} \left\{ \frac{1}{2} \|\nabla L * k - \nabla B\|_2^2 + \lambda \Phi(\nabla L, \Delta L) + \gamma \|k\|_2^2 \right\} \quad (2)$$

with $\lambda, \gamma > 0$ denoting the regularization parameters. The hybrid regularization term $\Phi(\nabla L, \Delta L)$ on image gradients is defined as $\Phi(\nabla L, \Delta L) = \alpha_1 \|\nabla L\|_0 + \alpha_2 \|\Delta L\|_0$ with $\alpha_1, \alpha_2 \in [0, 1]$ and $\alpha_1 + \alpha_2 = 1$. Here, $\|x\|_0$ counts the number of nonzero values of x . If $\alpha_2 = 0$, our proposed model (2) will simplify to a simple version introduced in [11]. Let ζ_1 and ζ_2 denote the magnitudes of the first and second-order differential operators, respectively. By considering the definitions of ∇ and Δ , it is easy to generate $\zeta_2 = \sqrt{2}\zeta_1$ [17]. We assume that the relationship between α_1 and α_2 could be roughly obtained from ζ_1 and ζ_2 . In this work, we propose an intuitive method to yield the relationship between α_1 and α_2 , i.e., $\alpha_2 = \sqrt{2}\alpha_1$. Thus, $\alpha_1 = \sqrt{2} - 1$ and $\alpha_2 = 2 - \sqrt{2}$ are selected in our experiments. In addition, our method does not take into account other additional operations, e.g., shock filtering [18, 19] or selecting informative edges [11, 19].

2.2. Numerical Optimization Algorithm

2.2.1. k -Estimation

In the blur kernel estimation step, given the fixed values of L_t , the blur kernel k at the $(t+1)$ -th outer iteration can be obtained by solving the least-squares optimization problem $k_{t+1} = \min_k \left\{ \frac{1}{2} \|\nabla L_t * k - \nabla B\|_2^2 + \gamma \|k\|_2^2 \right\}$, whose solution k_{t+1} is given by

$$k_{t+1} = \mathcal{F}^{-1} \left(\frac{\overline{\mathcal{F}(\nabla L_t)} \mathcal{F}(\nabla B)}{\overline{\mathcal{F}(\nabla L_t)} \mathcal{F}(\nabla L_t) + 2\gamma \mathbf{I}} \right), \quad (3)$$

where \mathbf{I} is an identity matrix, $\overline{(\cdot)}$ represents the complex conjugate operator, \mathcal{F} and \mathcal{F}^{-1} respectively denote the *Fast*

Fourier Transform (FFT) and its inverse version [11]. It is computationally efficient to generate the numerical solution.

2.2.2. ∇L -Estimation

Given the fixed value of k_{t+1} , the estimation of intermediate latent sharp image gradient ∇L at the $(t+1)$ -th outer iteration is equivalent to optimizing the following L0-regularized least-squares minimization problem

$$\nabla L_{t+1} = \min_{\nabla L} \left\{ \frac{1}{2} \|\nabla L * k_{t+1} - \nabla B\|_2^2 + \lambda \Phi(\nabla L, \Delta L) \right\} \quad (4)$$

To guarantee the solution stability, an ADMM-based numerical optimization algorithm [20] will be introduced to deal with (4). We first introduce two intermediate variables $Y = \nabla L$ and $Z = \Delta L$, then transform the unconstrained optimization problem (4) into a constrained formulation as follows

$$\begin{aligned} \min_{\nabla L, Y, Z} \left\{ \frac{1}{2} \|\nabla L * k_{t+1} - \nabla B\|_2^2 + \lambda (\alpha_1 \|Y\|_0 + \alpha_2 \|Z\|_0) \right\}, \\ \text{s.t. } Y = \nabla L, Z = \Delta L, \end{aligned} \quad (5)$$

whose augmented Lagrangian function can be formulated as $\mathcal{L}_{\mathcal{A}}(\nabla L, Y, Z; \xi, \varphi) = \frac{1}{2} \|\nabla L * k_{t+1} - \nabla B\|_2^2 + \lambda \alpha_1 \|Y\|_0 + \frac{\beta_1}{2} \left\| Y - \nabla L - \frac{\xi}{\beta_1} \right\|_2^2 + \lambda \alpha_2 \|Z\|_0 + \frac{\beta_2}{2} \left\| Z - \Delta L - \frac{\varphi}{\beta_2} \right\|_2^2$, where ξ and φ denote the Lagrangian multipliers, β_1 and β_2 are predefined positive parameters.

∇L -subproblem: At the $(s+1)$ -th inner iteration, the first ∇L -subproblem $\nabla L_{t,s+1} \leftarrow \min_{\nabla L} \mathcal{L}_{\mathcal{A}}(\nabla L, Y_s, Z_s; \xi_s, \varphi_s)$ can be handled by considering the following problem, i.e.,

$$\begin{aligned} \nabla L_{t,s+1} = \min_{\nabla L} \left\{ \frac{1}{2} \|\nabla L * k_{t+1} - \nabla B\|_2^2 \right. \\ \left. + \frac{\beta_1}{2} \left\| Y_s - \nabla L - \frac{\xi_s}{\beta_1} \right\|_2^2 + \frac{\beta_2}{2} \left\| Z_s - \Delta L - \frac{\varphi_s}{\beta_2} \right\|_2^2 \right\} \end{aligned} \quad (6)$$

for $s = 0, 1, \dots, S_{\max}$. The solution $\nabla L_{t,s+1}$ can be easily obtained using the forward and inverse FFT operators, i.e.,

$$\nabla L_{t,s+1} = \mathcal{F}^{-1} (\mathcal{F}_{\text{num}} / \mathcal{F}_{\text{den}}), \quad (7)$$

with $\mathcal{F}_{\text{den}} = \overline{\mathcal{F}(k)} \mathcal{F}(k) + \beta_1 \mathbf{I} + \beta_2 \overline{\mathcal{F}(\nabla)} \mathcal{F}(\nabla)$ and $\mathcal{F}_{\text{num}} = \overline{\mathcal{F}(k)} \mathcal{F}(\nabla B) + \beta_1 \mathcal{F}(Y_s - \frac{\xi_s}{\beta_1}) + \beta_2 \overline{\mathcal{F}(\nabla)} \mathcal{F}(Z_s - \frac{\varphi_s}{\beta_2})$.

(Y, Z) -subproblem: Given the fixed values of $\nabla L_{t,s+1}$, ξ_s and φ_s obtained from the previous iterations, the optimal solutions (Y_{s+1}, Z_{s+1}) of the (Y, Z) -subproblem $(Y_{s+1}, Z_{s+1}) \leftarrow \min_{Y, Z} \mathcal{L}_{\mathcal{A}}(\nabla L_{t,s+1}, Y, Z; \xi_s, \varphi_s)$ could be easily generated by implementing the L0-regularized least-squares minimization problems $Y_{s+1} = \min_Y \left\{ \frac{\beta_1}{2} \left\| Y - \left(\nabla L_{t,s+1} + \frac{\xi_s}{\beta_1} \right) \right\|_2^2 + \lambda \alpha_1 \|Y\|_0 \right\}$ and $Z_{s+1} = \min_Z \left\{ \frac{\beta_2}{2} \left\| Z - \left(\Delta L_{t,s+1} + \frac{\varphi_s}{\beta_2} \right) \right\|_2^2 + \lambda \alpha_2 \|Z\|_0 \right\}$ with $\nabla L_{t,0} = \nabla L_t$. The unknown variables Y

Algorithm 1 Robust Blur Kernel Estimation

- 1: **Input:** Blurred image B , $\tau = 1.618$, $\gamma = 5 \times 10^{-2}$, $\eta_1 = \eta_2 = 10^{-3}$, and $M_{\max} = 15$.
 - 2: **Initialize:** $k_0 = \text{uniform}$, $\nabla L_0 = \nabla B$ and $t = 0$.
 - 3: **while** (not converged and $t \leq T_{\max}$) **do**
 // Step 1 : *Blur Kernel Estimation* k_{t+1}
 - 4: Update k_{t+1} according to (3).
 // Step 2 : *Image Gradient Estimation* ∇L_{t+1}
 - 5: $\nabla L_{t,0} \leftarrow \nabla L_t$.
 - 6: **for** $s = 0$ to S_{\max} **do**
 - 7: Update $\nabla L_{t,s+1}$ according to (7).
 - 8: Update Y_{s+1} and Z_{s+1} according to (8) and (9).
 - 9: $\xi_{s+1} = \xi_s - \tau\beta_1 (Y_{s+1} - \nabla L_{t,s+1})$.
 - 10: $\varphi_{s+1} = \varphi_s - \tau\beta_2 (Z_{s+1} - \Delta L_{t,s+1})$.
 - 11: **end for**
 - 12: $\nabla L_{t+1} \leftarrow \nabla L_{t,S_{\max}}$.
 - 13: **end while**
 - 14: **Output:** blur kernel k .
-

and Z are componentwise separable. It is easy to generate the solutions Y_{s+1} and Z_{s+1} through the simple but effective element-wise hard-thresholding operator \mathcal{T} [21], i.e.,

$$Y_{s+1} = \mathcal{T}_{\lambda\alpha_1, \beta_1} (\nabla L_{t,s+1} + \xi_s / \beta_1), \quad (8)$$

$$Z_{s+1} = \mathcal{T}_{\lambda\alpha_2, \beta_2} (\Delta L_{t,s+1} + \varphi_s / \beta_2), \quad (9)$$

where $\mathcal{T}_{a,b}(x) = \text{sign}(\max(|x| - \sqrt{2a/b}, 0)) \circ x$ with $\text{sign}(\cdot)$ being sign function and \circ being pointwise product.

ξ and φ update: During each iteration, the Lagrange multipliers ξ and φ could be directly updated using $\xi_{s+1} = \xi_s - \tau\beta_1 (Y_{s+1} - \nabla L_{t,s+1})$ and $\varphi_{s+1} = \varphi_s - \tau\beta_2 (Z_{s+1} - \Delta L_{t,s+1})$ with $\tau = \frac{1+\sqrt{5}}{2}$. The reconstructed image gradient $\nabla L_{t+1} = \nabla L_{t,S_{\max}}$ is produced to assist in estimating blur kernel in the next step. The proposed numerical method is reasonable to handle the nonconvex nonsmooth L0-norm optimization problem (2). The whole optimization procedure is summarized in Algorithm 1.

3. LATENT SHARP IMAGE RESTORATION

To suppress outliers during non-blind deconvolution, the L1-norm data-fidelity term and edge-preserving TV regularizer were combined [19] to reconstruct the latent sharp image L . The TV-regularized variational model (i.e., TVL1) for non-blind deconvolution is given by

$$\min_L \{ \|L * k - B\|_1 + \mu \|\nabla L\|_1 \}, \quad (10)$$

where the regularization parameter μ is set to 5×10^{-2} . The L1-norm data-fidelity term in (10) commonly performs more robust to the undesirable outliers compared with the widely-used squared L2-norm version. The alternating minimization algorithm (AMA) was introduced to efficiently handle (10). More details could be found in [19].

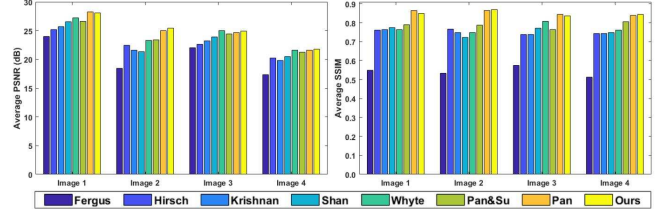


Fig. 1. Quantitative evaluation (left: PSNR, right: SSIM) on the benchmark dataset by [25] for different deblurring methods, i.e., Fergus [22], Hirsch [23], Krishnan [8], Shan [17], Whyte [24], Pan&Su [11], Pan [9] and our method.

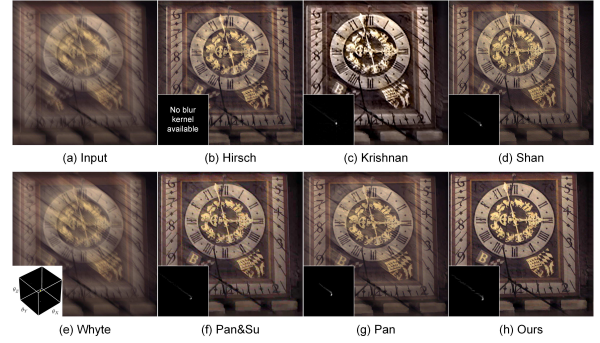


Fig. 2. Comparison with state-of-the-art deblurring methods on a synthetic image of size 800×800 . Our estimated (*uniform*) blur kernel of size 145×145 is visually illustrated in the bottom-left panel.

4. EXPERIMENTAL RESULTS AND DISCUSSION

Numerical experiments were performed using MATLAB R2017a on a machine with a 3.00 GHz Intel(R) Core (TM) i5-7400 CPU and 8.00 GB RAM. The experiments were implemented on both synthetic and realistic images to compare the proposed method with several state-of-the-art blind deblurring methods, i.e., Krishnan [8], Pan [9], Pan&Su [11], Shan [17], Fergus [22], Hirsch [23] and Whyte [24]. The first four methods were performed based on the *uniform* blur assumption. In contrast, the last two methods were able to handle *non-uniform* blurring situations. In all experiments, we manually selected the optimal parameters $\lambda = 2 \times 10^{-2}$, $\gamma = 1 \times 10^{-3}$, $\beta_1 = 5 \times 10^{-3}$, $\beta_2 = 1 \times 10^{-4}$, $\alpha_1 = \sqrt{2} - 1$ and $\alpha_2 = 2 - \sqrt{2}$ for our method. Experimental results have illustrated the effectiveness of these manually defined parameters. For the sake of fairness, online available implementations of the competing deblurring methods were used with the best tuning parameters and the best possible results.

4.1. Experiments on Synthetic Images

Synthetic experiments were conducted on the popular Köhler et al's benchmark dataset [25], which includes 48 blurred images (generated by 4 sharp images of size 800×800 and

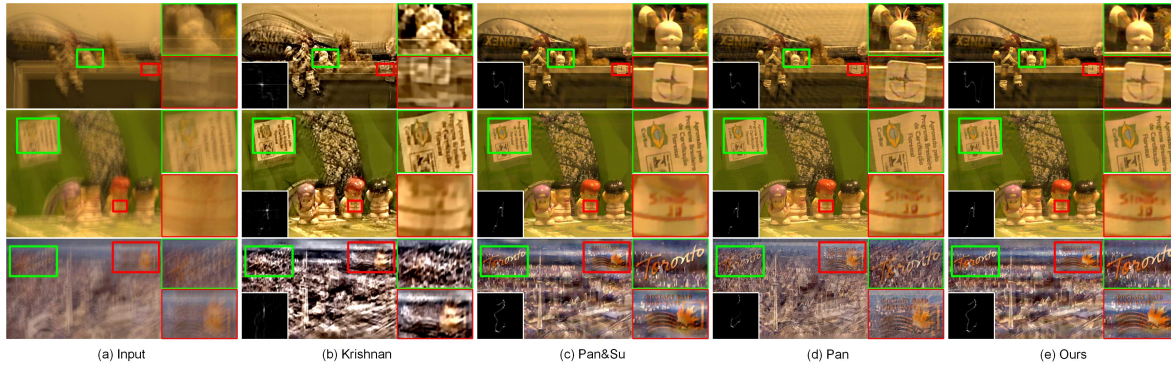


Fig. 3. Blind deblurring of three realistic natural images with large-scale blur kernels. The sizes of the estimated blur kernels from top to bottom are 135×135 , 101×101 and 95×95 , respectively. (The images are best viewed in full-screen mode.)

Table 1. Average computational time (Mean \pm Std) of Pan [9] and our method for four different images (Unit: minutes).

Methods	Image 1	Image 2	Image 3	Image 4
Pan [9]	11.6 ± 1.93	13.2 ± 2.37	13.0 ± 3.22	12.5 ± 2.21
Ours	0.84 ± 0.12	0.86 ± 0.17	0.89 ± 0.17	0.82 ± 0.11

12 different blur kernels). Both PSNR and SSIM metrics were selected to assess the competing deblurring methods. As shown in Fig. 1, our method was found to produce results comparable to the state-of-the-art blind deblurring methods in terms of average PSNR and SSIM values. In particular, the proposed method significantly outperforms Pan&Su [11] (*which could be considered as a special case of our method*) in all experiments. Its superior performance mainly benefits from the L0-regularized hybrid gradient sparsity priors. Pan [9] sometimes generates higher average PSNR and SSIM values by enforcing the sparsity of image dark channel. However, the deblurring performance suffers from extremely high computational cost shown in Table 1. Our proposed method is able to guarantee a good balance between deblurring quality and computational time. The good result of our method is further visually confirmed in Fig. 2. The competing methods easily cause significant artifacts in deblurred outputs. In contrast, our method could overcome the undesirable artifacts and improve the visual image quality.

4.2. Experiments on Realistic Images

This subsection only evaluates the imaging quality of *uniform* deblurring methods on several realistic blurred images. The natural images with large-scale blur kernels, shown in Fig. 3, were firstly selected to measure the deblurring performance. It is observed that our method is able to effectively estimate the large-scale blur kernels and reconstruct the latent sharp images. Pan [9] does not always perform well since the dark channel prior may sometimes fail to effectively represent the image sparsity property. Krishnan [8] easily generates inac-

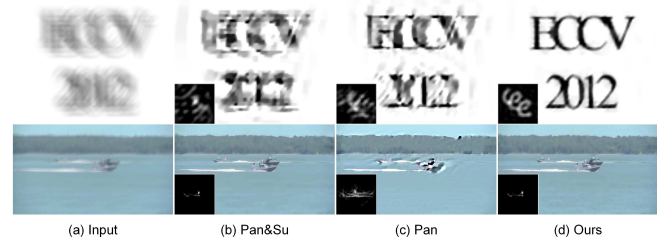


Fig. 4. Blind deblurring of two different realistic images. The sizes of the estimated blur kernels from top to bottom are 23×23 and 95×95 , respectively.

curate blur kernel estimations leading to poor image quality. Experiments on text image and ocean engineering were further implemented to evaluate the imaging performance. Deblurring results in Fig. 4 demonstrate that our method is able to generate superior performance for text image. In the field of ocean engineering, the proposed method performs favorably compared with the state-of-the-art deblurring methods. The structural features and fine details could be effectively preserved to enhance image quality. It can be concluded that the proposed L0-regularized hybrid gradient sparsity priors are beneficial for yielding accurate blur kernel estimation and improving final image quality.

5. CONCLUSIONS

To achieve high-quality blind deblurring, we proposed to introduce the L0-regularized hybrid gradient sparsity priors for robustly estimate blur kernels. The hybrid sparsity priors were able to preserve the gradient sparsity and salient edges, assisting in stabilizing the blur kernel estimation. Our estimation method does not need any other rigorous constraints on blur kernels and latent sharp images. The outlier-suppressing TVL1 model was then introduced to generate the final sharp images. Experiments have been performed to illustrate the good performance of our proposed method.

6. REFERENCES

- [1] C. Wang, Y. Yue, F. Dong, Y. Tao, X. Ma, G. Clapworthy, and X. Ye, "Enhancing Bayesian estimators for removing camera shake," *Comput. Graph. Forum*, vol. 32, no. 6, pp. 113-125, Mar. 2013.
- [2] A. Levin, Y. Weiss, F. Durand, and W. T. Freeman, "Understanding blind deconvolution algorithms," *IEEE TPAMI*, vol. 33, no. 12, pp. 2354-2367, Dec. 2011.
- [3] W. S. Lai, J. Huang, Z. Hu, N. Ahuja, and M. H. Yang, "A comparative study for single image blind deblurring," In *Proc. IEEE CVPR*, Las Vegas, Nevada, United States, Jun. 2016, pp. 1701-1709.
- [4] Y. Zhang and K. Hirakawa, "Combining inertial measurements with blind image deblurring using distance transform," *IEEE TCI*, vol. 2, no. 3, pp. 281-293, Sep. 2016.
- [5] J. Pan, Z. Hu, Z. Su, and M. H. Yang, " L_0 -regularized intensity and gradient prior for deblurring text images and beyond," *IEEE TPAMI*, vol. 39, no. 2, pp. 342-355, Feb. 2017.
- [6] S. D. Babacan, R. Molina, and A. K. Katsaggelos, "Variational Bayesian blind deconvolution using a total variation prior," *IEEE TIP*, vol. 18, no. 1, pp. 12-26, Jan. 2009.
- [7] D. Perrone and P. Favaro, "A logarithmic image prior for blind deconvolution," *Int. J. Comput. Vis.*, vol. 117, no. 2, pp. 159-172, Apr. 2016.
- [8] D. Krishnan, T. Tay, and R. Fergus, "Blind deconvolution using a normalized sparsity measure," In *Proc. IEEE CVPR*, Colorado Springs, CO, United States, Jun. 2011, pp. 233-240.
- [9] J. Pan, D. Sun, H. Pfister, and M. H. Yang, "Blind image deblurring using dark channel prior," In *Proc. IEEE CVPR*, Las Vegas, Nevada, United States, Jun. 2016, pp. 1628-1636.
- [10] Y. Yan, W. Ren, Y. Guo, R. Wang, and X. Cao, "Image deblurring via extreme channels prior," In *Proc. IEEE CVPR*, Honolulu, Hawaii, United States, Jul. 2017.
- [11] J. Pan and Z. Su, "Fast l_0 -regularized kernel estimation for robust motion deblurring," *IEEE Signal Process. Lett.*, vol. 20, no. 9, pp. 841-844, Sep. 2013.
- [12] L. Xu, S. Zheng, and J. Jia, "Unnatural l_0 sparse representation for natural image deblurring," In *Proc. IEEE CVPR*, Portland, Oregon, United States, Jun. 2013, pp. 1107-1114.
- [13] W. Z. Shao, H. B. Li, and M. Elad, "Bi- l_0 - l_2 -norm regularization for blind motion deblurring," *J. Vis. Commun. Image R.*, vol. 33, pp. 42-59, Nov. 2015.
- [14] W. Ren, X. Cao, J. Pan, X. Guo, W. Zuo, and M. H. Yang, "Image deblurring via enhanced low-rank prior," *IEEE TIP*, vol. 25, no. 7, pp. 3426-3437, Jul. 2016.
- [15] K. Papafitsoros and C. B. Schönlieb, "A combined first and second order variational approach for image reconstruction," *J. Math. Imaging Vis.*, vol. 48, no. 2, pp. 308-338, Feb. 2014.
- [16] G. Liu, T. Z. Huang, and J. Liu, "High-order TVL1-based images restoration and spatially adapted regularization parameter selection," *Comput. Math. Appl.*, vol. 67, no. 10, pp. 2015-2026, Jun. 2014.
- [17] Q. Shan, J. Jia, and A. Agarwala, "High-quality motion deblurring from a single image," *ACM Trans. Graph.*, vol. 27, no. 3, pp. 73, Aug. 2008.
- [18] J. H. Money and S. H. Kang, "Total variation minimizing blind deconvolution with shock filter reference," *Image and Vision Computing*, vol. 26, no. 2, pp. 302-314, Feb. 2008.
- [19] L. Xu and J. Jia, "Two-phase kernel estimation for robust motion deblurring," In *Proc. ECCV*, Heraklion, Crete, Greece, Sep. 2010, pp. 157-170.
- [20] S. Boyd, N. Parikh, E. Chu, B. Peleato, and J. Eckstein, "Distributed optimization and statistical learning via the alternating direction method of multipliers," *Foundations and Trends in Machine Learning*, vol. 3, no. 1, pp. 1-122, 2010.
- [21] B. Dong and Y. Zhang, "An efficient algorithm for l_0 minimization in wavelet frame based image restoration," *J. Sci. Comput.*, vol. 54, no. 2-3, pp. 350-368, Feb. 2013.
- [22] R. Fergus, B. Singh, A. Hertzmann, S. T. Roweis, and W. T. Freeman, "Removing camera shake from a single photograph," *ACM Trans. Graph.*, vol. 25, no. 3, pp. 787-794, Jul. 2006.
- [23] M. Hirsch, C. J. Schuler, S. Harmeling, and B. Schölkopf, "Fast removal of non-uniform camera shake," In *Proc. IEEE ICCV*, Barcelona, Spain, Nov. 2011, pp. 463-470.
- [24] O. Whyte, J. Sivic, and A. Zisserman, "Deblurring shaken and partially saturated images," *Int. J. Comput. Vis.*, vol. 110, no. 2, pp. 185-201, Nov. 2014.
- [25] R. Köhler, M. Hirsch, B. Mohler, B. Schölkopf, and S. Harmeling, "Recording and playback of camera shake: Benchmarking blind deconvolution with a real-world database," In *Proc. ECCV*, Firenze, Italy, Oct. 2012, pp. 27-40.